

The 2dF QSO Redshift Survey - IV. The QSO Power Spectrum from the 10k Catalogue

Fiona Hoyle^{1,*}, P. J. Outram¹, T. Shanks¹, S. M. Croom², B. J. Boyle²
N. S. Loaring³, L. Miller³ & R. J. Smith⁴,

¹ Department of Physics, Science Laboratories, South Road, Durham, DH1 3LE, U.K

² Anglo-Australian Observatory, PO Box 296, Epping, NSW 2121, Australia

³ Department of Physics, Oxford University, Keble Road, Oxford, OX1 3RH, UK

⁴ Liverpool John Moores University, Twelve Quays House, Egerton Wharf, Birkenhead, CH41 1LD

* email hoyle@venus.physics.drexel.edu

16 November 2018

ABSTRACT

We present a power spectrum analysis of the 10K catalogue from the 2dF QSO Redshift Survey. Although the Survey currently has a patchy angular selection function, we use the Virgo Consortium’s Hubble Volume simulation to demonstrate that we are able to make a useful first measurement of the power spectrum over a wide range of scales.

We compare the redshift-space power spectra of QSOs to those measured for galaxies and Abell clusters at low redshift and find that they show similar shapes in their overlap range, 50-150h⁻¹Mpc, with $P_{\text{QSO}}(k) \propto k^{-1.3}$. The amplitude of the QSO power spectrum at $z \approx 1.4$ is almost comparable to that of galaxies at the present day if $\Omega_m=0.3$ and $\Omega_\Lambda=0.7$ (the Λ cosmology), and a factor of ≈ 3 lower if $\Omega_m=1$ (the EdS cosmology) is assumed. The amplitude of the QSO power spectrum is a factor of ≈ 10 lower than that measured for Abell clusters at the present day. At larger scales, the QSO power spectra continue to rise robustly to ≈ 400 h⁻¹Mpc, implying more power at large scales than in the APM galaxy power spectrum measured by Baugh & Efstathiou.

We split the QSO sample into two redshift bins and find little evolution in the amplitude of the power spectrum, consistent with the result for the QSO correlation function. In models with $\Omega_m \gtrsim 0.1$ this represents evidence for a QSO-mass bias that evolves as a function of time.

We compare the QSO power spectra to CDM models to obtain a constraint on the shape parameter, Γ . For two choices of cosmology ($\Omega_m=1$, $\Omega_\Lambda=0$ and $\Omega_m=0.3$, $\Omega_\Lambda=0.7$), we find the best fit model has $\Gamma \approx 0.1 \pm 0.1$. In addition, we have shown that a power spectrum analysis of the Hubble Volume Λ CDM mock QSO catalogues with $\Gamma = 0.17$ as input, produces a result which is statistically consistent with the data. The analysis of the mock catalogues also indicates that the above results for Γ are unlikely to be dominated by systematic effects due to the current catalogue window. We conclude that the form of the QSO power spectrum shows large-scale power significantly in excess of the standard CDM prediction, similar to that seen in local galaxy surveys at intermediate scales.

Key words: surveys - quasars, quasars: general, large-scale structure of Universe, cosmology: observations

1 INTRODUCTION

Galaxy surveys have allowed us to study the large scale structure in the local Universe. Large clusters of galaxies

and voids have been detected in these surveys and they have placed constraints on cosmological parameters and models of structure formation. However, large area (> 100 deg²), galaxy redshift surveys have so far only probed cluster-

ing out to $z \lesssim 0.1$. Even the 2dF Galaxy Redshift Survey (Colless 1998) and the Sloan Digital Sky Survey (Gunn & Weinberg 1999) will only observe galaxies with redshifts $\lesssim 0.3$. Surveys such as the Canada-France Redshift Survey (Crampton et al. 1995) and the CNOC Survey (Yee et al. 2000) have probed galaxy clustering out past $z = 0.5$ and, in the future, the DEEP (Davis & Faber 1998) and VIR-MOS (Le Fèvre et al. 1998) Surveys will probe galaxy clustering out past $z \approx 1$. Steidel and collaborators have even developed techniques from which galaxies can be selected at higher redshifts by looking for the Lyman break (Steidel et al. 1995, 1999). However these deep surveys currently only cover a small area of sky and the resulting ‘pencil beams’ are unsuitable for direct power spectrum measurements. If we wish to measure the power spectrum of clustering out to high redshifts over a wide area in a reasonably short time period, then different techniques or a different class of object are required.

Since the work of Osmer (1981), redshift surveys of Quasi-Stellar Objects (QSOs) have been used to probe clustering at high redshifts. The initial attempts to measure QSO clustering proved inconclusive, due to the low number density of QSOs and the inhomogeneous nature of the surveys. However, it was demonstrated in the mid-1980’s that QSOs are clustered, at least on small $r < 10h^{-1}\text{Mpc}$ scales, and that the amplitude of QSO clustering is similar to that of present day, optically selected galaxies (Shaver 1984, Shanks et al. 1986, 1987). More recently, several groups have looked at the evolution of QSO clustering. Croom & Shanks (1996) found that the amplitude of QSO clustering remains approximately constant with redshift, whereas La Franca, Andreani & Cristiani (1998) found that the clustering amplitude of optically bright QSOs evolves slowly with redshift, such that the clustering amplitude of high redshift QSOs is 2σ higher than that of low redshift QSOs. However, existing surveys of QSOs are still fairly small, for example, the Durham/AAT Survey (Boyle 1986) contains ≈ 400 QSOs and Large Bright QSO Survey (Hewitt, Foltz & Chaffee 1995) contains 1,053 QSOs. Measurements of some clustering statistics have been hampered by the small number of objects contained in the survey or the limited sky coverage of the surveys.

Our knowledge of the structure of the Universe at high redshifts will be drastically improved once the 2dF QSO Redshift Survey (2QZ, Croom et al. 1998; Boyle et al. 2000; Croom et al. 2001) and the QSO part of the Sloan Digital Sky Survey (Gunn & Weinberg 1995) are finished. These surveys will contain at least a factor of 25 more QSOs and cover a larger area of sky than existing QSO surveys. One of the key aims of both surveys is to measure the clustering of QSOs out to $\approx 1000h^{-1}\text{Mpc}$ with greater accuracy than is possible with existing surveys. For example, the increased number of QSOs in the 2dF QSO survey should reduce the errors on the measured correlation function by at least a factor of 5 on scales $\gtrsim 10h^{-1}\text{Mpc}$ (Croom et al. 2001)

The power spectrum is now established as one of the favoured methods of quantifying clustering. (Baugh & Efstathiou 1994; Tadros & Efstathiou 1996; Lin et al. 1996; Hoyle et al. 1999). One advantage of the power spectrum over the two-point correlation function is that the two-point correlation function is affected by uncertainties in the mean density on all scales, whereas the power spectrum is only

affected by these uncertainties on the largest scales (Cole, Fisher & Weinberg 1995). Ideally, we would like to measure the power spectrum of the mass density field, as this is the statistic predicted by models of structure formation. However, we are only able to observe the light in the Universe. Therefore, we generally measure the power spectrum of objects such as galaxies, clusters and QSOs, although there are promising methods for measuring the mass power spectrum from Lyman alpha forest systems (Croft et al. 1998) and from weak lensing (Wilson, Kaiser & Luppino 2001).

However, if the bias is scale independent, then although the amplitude of the QSO power spectrum may be different to that of the mass, the form of the QSO power spectrum will directly probe the shape of the mass power spectrum; the assumption of scale independent bias may be more appropriate at large scales (Coles 1993; Mann, Peacock & Heavens 1998).

The power spectrum has never before been measured from optically selected QSOs. QSOs are detected out to high redshifts and so QSO surveys have a large volume. However, existing surveys only cover small areas of sky and contain only a small number of QSOs. The survey geometry and low QSO number density within the surveys would have severely restricted the range of scales over which the power spectrum could have been reliably measured.

In this paper, we apply a power spectrum analysis to the 10k release catalogue. A correlation function analysis of the identical sample has been performed by Croom et al. (2000). We describe the current data set in Section 2 and look at the angular distribution of the QSOs in order to create the random catalogues needed in the power spectrum analysis. In Section 3 we briefly describe the method of power spectrum analysis and in Section 4 we test the measurement of the power spectrum from the current survey window using mock catalogues drawn from the Virgo consortiums *Hubble Volume* lightcone simulation (Frenk et al. 2000). In Section 5 we compare the QSO power spectrum to power spectra of present day galaxies and clusters and we see how the QSO power spectrum evolves with redshift. In Section 6 we compare the QSO power spectrum with power spectra of models of large scale structure and in Section 7 we draw our conclusions.

2 THE 10K CATALOGUE

In this paper, we analyse QSOs that will be contained in the first public release of the 2QZ, known as the *10k Catalogue*. The catalogue will contain 10681 QSOs and will be released to the community in the first half of 2001. This catalogue will contain the most spectroscopically complete fields (i.e. fields in which more than 85 per cent of objects have been identified) that were observed prior to November 2000. It will eventually be available from www.2dfquasar.org.

QSO candidates are identified from broad band ub_Jr colours from Automatic Plate Measuring (APM) facility measurements of UK Schmidt Telescope (UKST) photographic plates. This colour selection gives a photometric completeness of better than 90 per cent up to $z \approx 2.2$ (Boyle et al. 2000). The spectra of the objects are obtained using the 2dF instrument on the AAT. The spectra are reduced using the 2dF pipeline reduction system (Bailey & Glazebrook

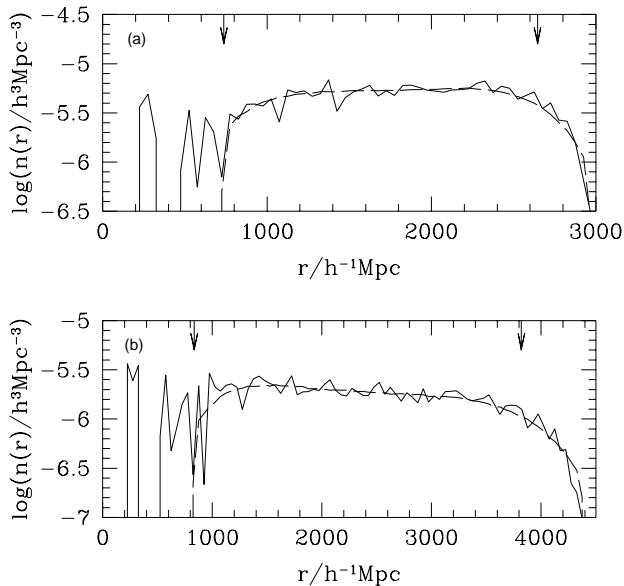


Figure 1. The radial number density of QSOs in bins of $\Delta r = 50h^{-1}\text{Mpc}$ in the SGC (solid line) calculated assuming EdS (a) and Λ (b). The dashed lines show the number density as measured from the random catalogues, normalised to match the number density of the QSOs. The number density varies slowly as a function of scale, decreasing only by a factor of approximately three over the range $0.3 < z < 2.2$, indicated by the arrows. At higher redshifts, the number density decreases rapidly.

1999) and objects are identified as QSOs by an automated procedure known as AUTOZ (Miller et al. 2001). AUTOZ also identifies the QSO redshifts; these have also been visually checked by two independent observers.

Observations have been made over two $5 \times 75 \text{ deg}^2$ strips in the North and South Galactic Cap regions. The North Galactic Cap strip is centred at $\delta = 0^\circ$ with $09^{\text{h}}50^{\text{m}} \lesssim \alpha \lesssim 14^{\text{h}}50^{\text{m}}$, while the South Galactic Cap strip is centred at $\delta = -30^\circ$, with $21^{\text{h}}40^{\text{m}} \lesssim \alpha \lesssim 03^{\text{h}}15^{\text{m}}$. We will refer to these regions as the NGC and SGC respectively. The finished survey will cover an area of 740 deg^2 . See Croom (1997), Smith (1998) and Smith et al. (2001) for further details of the photometric catalogue.

For each QSO, we have an angular position and a redshift. In order to convert from a redshift into a comoving distance, we need to adopt a cosmology. We consider an $\Omega_{\text{m}}=1.0$, $\Omega_{\Lambda}=0.0$ cosmology (EdS hereafter) and an $\Omega_{\text{m}}=0.3$, $\Omega_{\Lambda}=0.7$ cosmology (referred to as the Λ cosmology hereafter). Other cosmologies, such as open cosmologies, could also be considered but here we restrict our analysis to flat cosmologies, consistent with the recent results from balloon experiments such as Boomerang (de Bernardis et al. 2000) and Maxima (Balbi et al. 2000).

2.1 Constructing the Random Catalogue

2.1.1 The Radial Selection Function

The power spectrum measured directly from a QSO redshift survey is a convolution of the power spectrum of QSO clustering with the power spectrum of the survey geometry. In order to estimate the power spectrum of the survey

geometry, or window function, we generate a catalogue of random points which have the same angular and radial selection function as the QSOs but otherwise are unclustered.

Redshifts are drawn at random according to a 6th order polynomial $N(z)$ fit over the range of redshift and geometry of the sample under consideration. Using an approximation to the true $N(z)$ distribution can remove some of the large scale power. We test this by creating a 10th order polynomial $N(z)$ fit and remeasure the Λ cosmology power spectrum. Out to scales of $200h^{-1}\text{Mpc}$ ($\log(k/h \text{ Mpc}^{-1}) > -1.5$) the two power spectra are virtually indistinguishable. At $400h^{-1}\text{Mpc}$ ($\log(k/h \text{ Mpc}^{-1}) > -1.8$), the power spectra agree in amplitude to within 15%. The fractional error at this scale is 40% so the difference is negligible compared to the errors. The Survey geometry is also limiting how accurately the power spectrum can be measured on these scales too. (See Section 4 for details of the window function tests.)

Figure 1 shows the radial selection function of QSOs in the SGC (solid line) and in the random catalogue (dashed line) assuming EdS (a) and assuming the Λ cosmology (b). Over a wide range of redshift the selection function of the random catalogue accurately reproduces that of the QSOs. The radial selection function of the QSOs only varies slowly as a function of scale over the range of redshifts $0.3 < z < 2.2$, indicated by the arrows. The value of $n(r)$ changes by only a factor of ≈ 3 over the range of scales corresponding to $0.3 < z < 2.2$, whereas the value of $n(r)$ for galaxies changes by a far greater factor over a far smaller range of scales (for example see Figure 2 in Hoyle et al. 1999). This is because the luminosity evolution approximately cancels the effect of luminosity distance so we are always surveying the luminosity function to approximately the same absolute magnitude, relative to the break, M_B^* , almost independent of redshift. As it is desirable to have a constant number density when measuring clustering statistics to remove the need for a weighting scheme (other than giving all QSOs equal weight), we restrict the QSOs in our sample to have redshifts in the range $0.3 < z < 2.2$. This gives us a sample of 8935 QSOs.

2.1.2 The Angular Selection Function

Observations have been made across both the NGC and SGC strips. An optimal tiling algorithm for the 2dF Galaxy Redshift survey was developed by the 2dF Consortium to allow as many galaxies and QSOs as possible to be observed in each pointing. Pointings also overlap in high density regions to maximise the coverage in all areas of the survey. Therefore, the 10k catalogue has a patchy angular selection function, as can be seen in Figure 1. of Croom et al. (2001), which has to be matched by the random catalogue.

To match the angular selection function of the QSOs, we construct a completeness map. In each region defined by the intersection of 2dF pointings we calculate the number of objects observed and divide this by the number of candidates within that region to define the fractional observational completeness. This allows us to estimate the completeness in areas where two or more 2dF fields overlap. The completeness map is then rebinned to $1' \times 1'$ bins and the number of random points in each bin is weighted by this fractional completeness.

We also account for the extinction due to galactic dust

as this changes the effective magnitude limit of the survey as a function of position. We use the estimate of the dust reddening, $E(B-V)$, as a function of position given by Schlegel, Finkbeiner & Davis (1998) and weight the random distribution by

$$W_{\text{ext}}(\alpha, \delta) = 10^{-\beta A_{b_j}} \quad (1)$$

where $A_{b_j} = 4.035E(B-V)$ and $\beta = 0.3$, the slope of the QSO number counts at the magnitude limit of the survey, $b_j=20.85$. We have measured the power spectrum using random catalogues that were constructed with or without taking into account the effect of dust. We find that dust has a less than 5% effect on the power spectrum amplitude out to scales of $300h^{-1}\text{Mpc}$ ($\log(k/h \text{Mpc}^{-1}) > -1.7$) for the EdS cosmology, $400h^{-1}\text{Mpc}$ ($\log(k/h \text{Mpc}^{-1}) > -1.8$) for the Λ cosmology.

One further effect that could influence the shape of the power spectrum on large scales is due to possible errors in the zero-point calibration of the UKST plates. A conservative estimate of the current uncertainty is $\approx 0.2 \text{ mag}$ (Smith et al. 2001), although further CCD photometry is currently being obtained and we expect that the uncertainty in the zero-point calibration will be considerably lower in the final catalogue.

With a QSO number count slope of $\beta=0.3$, a 0.2 mag change in the zero-point calibration would change the expected QSO number density by ≈ 15 per cent. To estimate the effect this has on the QSO power spectrum, we generate different realisations of the random catalogues including plate-to-plate variations in the zero-point calibration. These are introduced by randomly varying the number density of points in the random catalogue on each UKST plate by r.m.s. 15 per cent. The uncertainty this introduces into the QSO power spectrum estimate is then given by the dispersion in the power spectra obtained from each realisation. We find that the fractional error introduced by this uncertainty varies between 1 and 5 per cent up to scales of $300h^{-1}\text{Mpc}$ or $\log(k/h \text{Mpc}^{-1}) > -1.7$ ($400h^{-1}\text{Mpc}$ or $\log(k/h \text{Mpc}^{-1}) > -1.8$ in the Λ case), where the QSO power spectrum can be robustly measured. On these scales the fractional FKP errors (discussed below) are ≈ 30 per cent, and therefore the total error is increased by $\lesssim 1\%$, less than the potential systematic error.

In Figure 2 we show the window function of the current 2QZ in the SGC (solid line) compared to the *expected* window function of a finished $5 \times 75 \text{ deg}^2$ strip (dashed line) calculated assuming EdS (a) and Λ (b). The window function of the NGC is very similar in slope and amplitude as although more QSOs have been observed on the SGC strip, the QSOs in the NGC are evenly distributed across the $5 \times 75 \text{ deg}^2$ strip (see Figure 1 Croom et. al 2001b). Both window functions are steep power laws, proportional to k^{-4} out to scales of $\approx 300h^{-1}\text{Mpc}$ ($\log(k/h \text{Mpc}^{-1}) > -1.7$) EdS or $\approx 400h^{-1}\text{Mpc}$ ($\log(k/h \text{Mpc}^{-1}) > -1.8$) for the Λ cosmology. When the survey is finished, the power laws will extend to $\approx 500h^{-1}\text{Mpc}$ ($\log(k/h \text{Mpc}^{-1}) > -1.9$) EdS, $600h^{-1}\text{Mpc}$ ($\log(k/h \text{Mpc}^{-1}) > -1.98$) for the Λ cosmology (see Hoyle 2000). We conclude that geometric effects (dust, plate-to-plate variations in the zero points, window function of the survey) do not effect the shape of the QSO power spectrum on scales $\lesssim 300h^{-1}\text{Mpc}$ ($\log(k/h \text{Mpc}^{-1}) > -1.7$) assuming

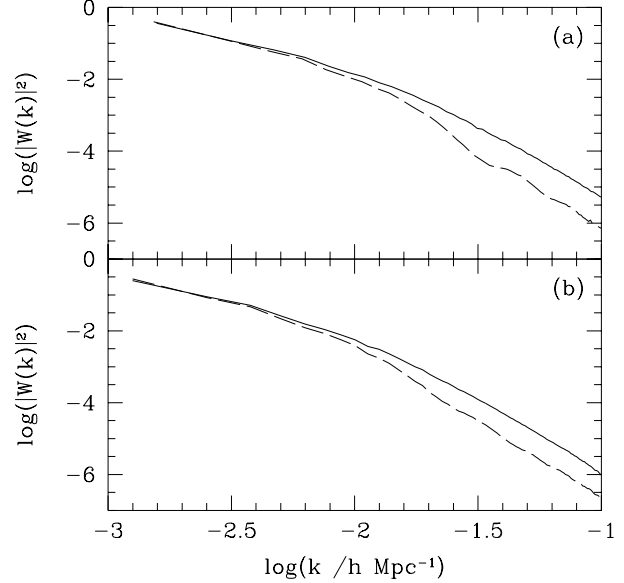


Figure 2. The window function of the current 2QZ in the SGC (solid line) compared to the *expected* window function of a finished $5 \times 75 \text{ deg}^2$ strip (dashed line) calculated assuming EdS (a) and Λ (b). The window function of the NGC is very similar to that of the SGC and both are a steep power law out to scales of $\approx 300h^{-1}\text{Mpc}$ ($\approx 400h^{-1}\text{Mpc}$ for the Λ cosmology) as opposed to $\approx 450h^{-1}\text{Mpc}$ ($600h^{-1}\text{Mpc}$) when the survey is finished.

the EdS cosmology $\lesssim 400h^{-1}\text{Mpc}$ ($\log(k/h \text{Mpc}^{-1}) > -1.8$) for the Λ cosmology.

3 MEASURING THE QSO POWER SPECTRUM

3.1 Power Spectrum Estimation

The power spectrum estimator that we adopt is similar to that given Tadros & Efstathiou (1996) and the same as that given in Hoyle et al. (1999). We outline the details below.

The Fourier transform of the observed QSO density field, within a periodic volume V , is given by

$$\hat{n}_e(\mathbf{k}) = \frac{1}{V} \sum_i e^{i\mathbf{k} \cdot \mathbf{x}_i(\mathbf{r})}. \quad (2)$$

where the $\mathbf{x}_i(\mathbf{r})$ refer to the spatial positions of the QSOs. The Fourier transform of the survey window function is approximated by:

$$\hat{W}_e(\mathbf{k}) = \frac{1}{V} \sum_i e^{i\mathbf{k} \cdot \mathbf{x}_i(\mathbf{r})}, \quad (3)$$

where this time the $\mathbf{x}_i(\mathbf{r})$ refer to the spatial positions of the random points (cf equations 7, 8 and 9 of Tadros & Efstathiou 1996 and equations 3 and 4 in Hoyle et al. 1999). Due to the large number of unclustered random points used, shot noise makes a negligible contribution to this estimate. The power spectra of the survey window function, shown in Figure 2, are much steeper than the expected QSO power spectrum, falling off as $\propto k^{-4}$ for wavenumbers $\log(k/h \text{Mpc}^{-1}) > -1.7$ or scales of $300h^{-1}\text{Mpc}$ in the EdS case ($\log(k/h \text{Mpc}^{-1}) > -1.8$ or scales of $400h^{-1}\text{Mpc}$

in the Λ case). Therefore the main effect of the convolution with the survey window function is to alter the shape of the power spectrum only on scales larger than $300h^{-1}\text{Mpc}$, $\log(k/h\text{Mpc}^{-1}) > -1.7$, ($400h^{-1}\text{Mpc}$, $\log(k/h\text{Mpc}^{-1}) > -1.8$ assuming the Λ cosmology).

Following Tadros & Efstathiou, we define a quantity with a mean value of zero:

$$\delta(\mathbf{k}) = \hat{n}_o(\mathbf{k}) - \alpha \hat{W}_e(\mathbf{k}), \quad (4)$$

where α is the ratio of the number of QSOs to random points in samples with constant number density. The power spectrum of QSO clustering is then estimated using:

$$P_e(k) = \left[\frac{1}{N_{\text{ran}}^2} \frac{1}{V} \sum_{k'} \left(V^2 |W_e(k')|^2 - \frac{1}{N_{\text{ran}}} \right) \right]^{-1} \times \left(\frac{V^2 |\delta(k)|^2}{N_{\text{QSO}}^2} - \frac{1}{N_{\text{QSO}}} - \frac{1}{N_{\text{ran}}} \right). \quad (5)$$

We use a Fast Fourier Transform (FFT) to compute the power spectrum and bin the Fourier modes up logarithmically to reduce the covariance between each bin.

The limit beyond which a power spectrum cannot be measured using a FFT is known as the Nyquist frequency. This is the frequency at which the grid samples the wave exactly twice per cycle:

$$k_{\text{Nyq}} = \frac{1}{2} \frac{2\pi}{\Delta}, \quad (6)$$

where, for a 256^3 FFT and a box of size $5000h^{-1}\text{Mpc}$, the interval $\Delta=5000/256h^{-1}\text{Mpc}$. The limit out to which the power spectrum measurement is reliable depends on the grid assignment scheme, and is a fraction of k_{Nyq} . Using the nearest grid point assignment scheme, $k_{\text{lim}} \approx 1/2 k_{\text{Nyq}}$ (Hatton 1999), which, for the above box size, corresponds to a value of $\log(k_{\text{lim}}) \approx -1$ or a scale of $\approx 60h^{-1}\text{Mpc}$.

To enable measurements of the power spectrum on smaller scales, we use a direct method of computing the Fourier transform. This method is time intensive and can only be applied to a small number of particles (so cannot be applied to the random catalogue). For the direct method, we make the assumption that equation 4 can be rewritten as $\delta(\mathbf{k}) = \hat{n}(\mathbf{k})$, which is only valid on small scales where the window function has a small amplitude (Figure 2). Using mock catalogues drawn from the *Hubble Volume* simulation (see Section 4), we find that on scales smaller than $\approx 100h^{-1}\text{Mpc}$ ($\log(k) \approx -1.2$) this approximation is accurate.

3.2 Error Determination

The errors on the power spectrum are estimated using the method of Feldman, Kaiser & Peacock (1994), equation 2.3.2, assuming that all QSOs carry equal weight when estimating the QSO power spectrum. The error is given by

$$\frac{\sigma^2(k)}{P^2(k)} = \frac{(2\pi)^3 [1 + \frac{1}{n(r)P(k)}]^2}{V_k V_s} \quad (7)$$

where V_k is the volume of each bin in k -space, estimated by $V_k = N_k(\Delta k)^3$ with N_k the number of independent modes in the k -shell and $(\Delta k)^3$ the volume of one k -mode. V_s is the

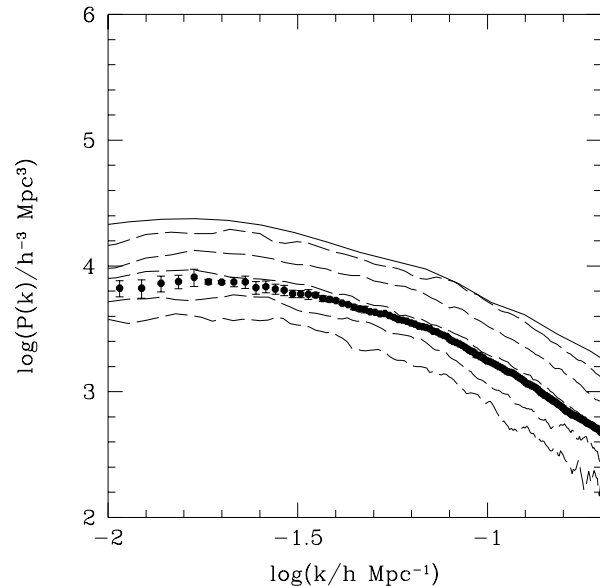


Figure 3. The solid line shows the input power spectrum to the *Hubble Volume* simulation. The dashed lines show power spectra of the mass in the simulation in bins of 0.5 in redshift, centred on (reading down) 0.25, 0.75, 1.25, 1.75 and 2.25. The points show the power spectrum of the mass in the light cone out to $z < 2.4$. The amplitude of this power spectrum is close to the amplitude of the power spectrum at the average redshift of the sample which is $\bar{z} = 1.4$.

volume of the survey. Over a wide range of scales these errors are found to be in reasonable agreement with errors estimated from the dispersion over power spectrum estimates from the *Hubble Volume* mock catalogues (see Section 4 and Hoyle 2000). On the smallest scales, the FKP errors appear smaller than those from the mock catalogues. FKP errors are only valid in the fully linear regime and non-linearities on small scales may mean they underestimate the true error on these scales Meiksin & White (1999).

To obtain a single 2QZ power spectrum for each assumed cosmology, we average the power spectrum of the QSOs in the NGC and SGC together, weighting by the inverse of the variance on each scale.

4 TESTING P(K) ESTIMATORS USING THE HUBBLE VOLUME

To test the estimator of the power spectrum and the effect of the window function on the recovered power spectrum, we have constructed mock catalogues that approximately match the clustering and geometry expected from the final QSO sample. Full details of the mock catalogues can be found in Hoyle (2000). We review the features most pertinent to the analysis here.

The mock catalogues are constructed from the Virgo consortium's *Hubble Volume* simulation (see Frenk et al. 2000). The simulation has a ΛCDM cosmology with $\Omega_m=0.3$, $\Omega_b=0.04$ and $\Omega_\Lambda=0.7$, $h=0.7$ and normalised to $\sigma_8=0.9$ at present day and with shape parameter of $\Gamma = 0.17$. The simulation has a lightcone output such that the evolution of the dark matter is fully accounted for. It extends to redshift ≈ 4 ,

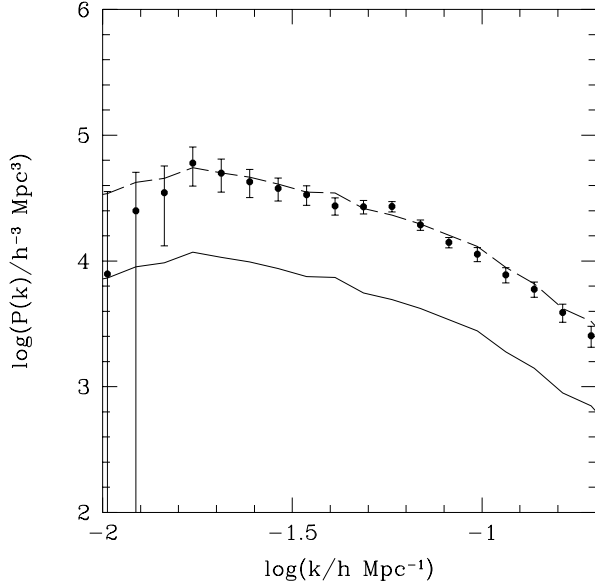


Figure 4. The points show the power spectrum measured from the biased mock catalogues, the solid line shows the mass power spectrum and the dashed line shows the mass power spectrum multiplied by a factor of $b^2=4.7$. Both the mass and the biased catalogues have the selection function of the QSOs imprinted on them and are measured in redshift space.

and covers an area of $15 \times 75 \text{deg}^2$, which we split into three $5 \times 75 \text{deg}^2$ strips to match the geometry of the 2QZ strips. The three strips are not entirely independent so when we imprint the NGC and SGC completeness maps (see later in this section) on the simulations, we just consider the outer slices.

The simulation has a lightcone output such that the evolution of the dark matter is fully accounted for. However, in Figure 3 we show that evolution has little effect on the shape of the mass power spectrum on the scales where it can be robustly measured. The solid line is the input power spectrum to the *Hubble Volume* simulation. The dashed lines show the power spectra of the mass in the simulation in bins of 0.5 in redshift centred on (reading down) 0.25, 0.75, 1.25, 1.75 and 2.25. The points show the power spectrum of the mass over the light cone out to $z < 2.5$, the average redshift of the mass is $z \approx 1.4$. This power spectrum does indeed lie between the power spectra centred on $z = 1.25$ and $z = 1.75$ and all three power spectra have very similar shapes.

We bias the dark matter particles to approximately match the clustering expected from 2QZ. Initial measurements of the correlation function suggested that the correlation length of the 2QZ QSOs would be $\approx 6h^{-1} \text{Mpc}$, assuming the Λ cosmology, and that the comoving correlation length would be roughly constant with redshift. See Croom et al. (2001) for the latest measurements of the correlation function.

The biasing prescription is described in full detail in Hoyle (2000). We provide a brief summary here. We split the simulation into slices of 0.2 in redshift. Within each slice, we bin the redshift space density field onto a grid of cell size $20h^{-1} \text{Mpc}$ and calculate the mean density and standard

deviation for each cell. Following Cole et al. (1998), the bias probability is given by

$$P(\nu) = \begin{cases} \exp(\alpha\nu + \beta\nu^{3/2}) & \text{if } \nu \geq 0 \\ \exp(\alpha\nu) & \text{otherwise,} \end{cases} \quad (8)$$

where ν is the number of standard deviations of the cell density away from the mean cell density. We fix α to be 0.15, similar to the value given in Cole et al. such that the real space clustering at present day in a Λ CDM simulation with parameters similar to those of the *Hubble Volume* approximately matches that of the APM galaxy survey (Baugh & Efstathiou 1993). We vary β until the correlation length of biased particles in each redshift slice is consistent with $6h^{-1} \text{Mpc}$ over the range $5 < r < 30h^{-1} \text{Mpc}$, assuming that the correlation function has the form $\xi(r) = (r/r_0)^{-1.7}$.

As the clustering amplitude of the dark matter decreases with redshift proportional to the square of the linear growth factor, the bias factor required to keep the clustering amplitude constant with redshift must correspondingly increase with redshift, proportional to the growth factor. At the average redshift of the survey, the bias factor, b , is approximately $\sqrt{4.7}$. We then imprint the radial selection function of the QSOs onto the mock catalogues as described in Section 2.1.

The net result is shown in Figure 4. The points show $P(k)$ for the biased particles, the solid line shows $P(k)$ of the mass and the dashed line shows $b^2 P(k)_{\text{mass}}$. In both cases, the QSO selection function has been applied to the catalogues and the redshift space distortions included in the particle positions. By design, over a wide range of scales, there is just a linear bias between the mass and the biased particles.

In Figure 5, we test the method of estimating the power spectrum on the mock catalogues of the finished 2QZ. The solid line shows the input power spectrum to the *Hubble Volume* simulation. The power spectra from 2QZ and the mock catalogues are measured in redshift space, whereas the input power spectra is calculated in real space. Small scale peculiar velocities affect the shape of the redshift power spectrum on small scales. However, they should have little effect on the shape of the power spectrum on scales $\gtrsim 5h^{-1} \text{Mpc}$ (see Hoyle 2000), which is below the scale where we can measure QSO power spectra.

On large scales, the effect of redshift space distortions is to boost the amplitude of the power spectrum according to

$$P_s(k) = P_r(k) \left(1 + \frac{2}{3}\beta + \frac{1}{5}\beta^2 \right), \quad (9)$$

(Kaiser 1987) with $\beta = \Omega_m^{0.6}/b$ and r and s indicating the real space and redshift space power spectra. The redshift space distortions are caused by bulk motions of QSOs. If the bias is scale independent the redshift space power spectrum just has a higher amplitude than the real space power spectrum but the shapes should be consistent. Therefore we test our method of recovering the power spectrum by comparing to the shape of the input power spectrum.

The circles in the left plot show the power spectrum from the mock catalogues, averaged over the three realisations, estimated using a FFT. On intermediate to large scales, ($60\text{-}400h^{-1} \text{Mpc}$ or $-1.8 < \log(k) < -1$) the power spectrum from the mock catalogues using the FFT repro-

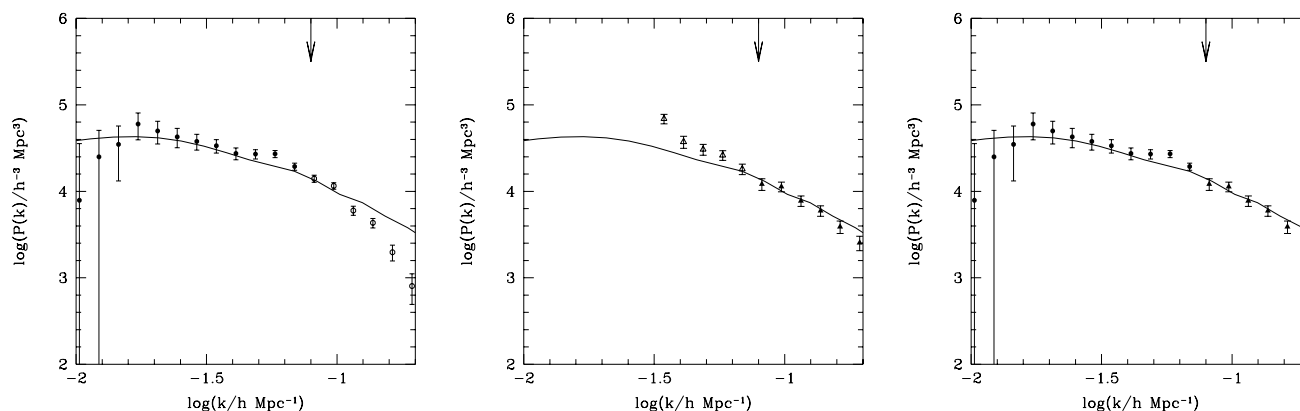


Figure 5. The circles in the left panel show the power spectrum from the mock catalogues of the finished 2QZ found using a FFT. The triangles in the middle plot show the power spectrum from the mock catalogues using the direct Fourier Transform method. In the right plot, the circles show the mock catalogue power spectrum, estimated using a FFT on scales above the arrow and the direct method on scales below the arrow. In all cases, the line shows the real space input power spectrum to the *Hubble Volume* simulation, renormalised to mimic the effects of bulk motions on the power spectrum amplitude. The open symbols demonstrate the points affected by problems with each different method of power spectrum estimation. On small scales, the open circles lie below the input power spectrum as these scales are below the FFT limit. On large scales, the open triangles lie above the input power spectrum as we have not accounted for the window function normalisation. A combination of the two methods gives a good match to the input power spectrum over a wide range of scales, as seen in the right hand plot.

duces the shape of the input power spectrum very well. On the very largest scales, the points are systematically below the line due to the effects of the window function. A convolution of the input power spectrum with the window function reveals a very similar decrease in power on these large scales (Hoyle 2000). It is very difficult to deconvolve fully the window function from the true power spectrum. Instead of attempting this, we estimate the scale on which the window function affects the shape of the power spectrum through comparisons with the input power spectrum. Assuming the Λ cosmology, the power spectrum will be free from any effects of the window function on scale less than $400h^{-1}\text{Mpc}$ ($\log(k/h\text{Mpc}^{-1})=-1.8$). On small scales, the circles lie below the input power spectrum. These scales are below the limit of the FFT and the power spectrum cannot be robustly measured.

Instead, on small scales we use a direct Fourier transform to calculate the power spectrum. This is shown by the triangles in the middle plot. The solid triangles reproduce the input power spectrum well on scales smaller than $\approx 100h^{-1}\text{Mpc}$ ($\log(k/h\text{Mpc}^{-1})=-1.2$) where the window function has little effect on the amplitude of the power spectrum. On larger scales, the effect of not subtracting off the window function in the estimation of the power spectrum can clearly be seen.

In the right hand plot, we show a combination of the two methods. On scales larger than the arrow, we use the FFT method and on scales smaller than the arrow, we use the direct method. This enables a robust measurement of the power spectrum over a wide range of scales. The scale at which we swap the method of estimating the power spectrum is the central point at which the two methods of estimating the power spectrum agree within the 1σ errors.

The 2QZ is, however, not yet finished and currently has a patchy angular selection function, as discussed in section 2.1.2. To test the effect of this on the power spectrum, we imprint the angular selection function of the NGC and SGC

onto the two outer mock catalogues, as described in Section 2.1.2. Figure 6(a) shows the average power spectrum after the angular selection function of the NGC (filled circles) and the SGC (open circles) has been imprinted onto the mock catalogues.

In Figure 6(b), we combine the power spectrum of the NGC and SGC together, weighted by the inverse of the variance, to create one single mock 2QZ power spectrum. The same combination of FFT and direct Fourier Transform, as described above, was used in the calculation of the power spectrum.

Over the range of values $-1.8 < \log(k) < -1$ ($60-400h^{-1}\text{Mpc}$), the power spectrum from the NGC and SGC mock catalogues and the combined power spectrum match the input power spectrum reasonably well although there is, perhaps, a slight steepening of the power spectrum. On larger and smaller scales, the agreement between the mock power spectra and the input power spectrum worsens compared to the agreement between the mock, finished power spectrum and the input power spectrum. This is due to the smaller volume of the incomplete survey, the smaller number of QSOs currently observed and errors that, through tests on the *Hubble Volume* (see Section 3.2 and Hoyle 2000), are perhaps underestimated using the FKP method.

The tests show that even with the incomplete 2QZ, accurate measurements of the power spectrum can be made, although over a slightly limited range of scales as compared to the power spectrum predicted from the final survey, with errors that are larger (by a factor of ≈ 1.5) than the finished survey will have.

5 RESULTS

5.1 The QSO Power Spectra

In this Section, we present QSO power spectra measured from the NGC, SGC as well as the combined power spec-

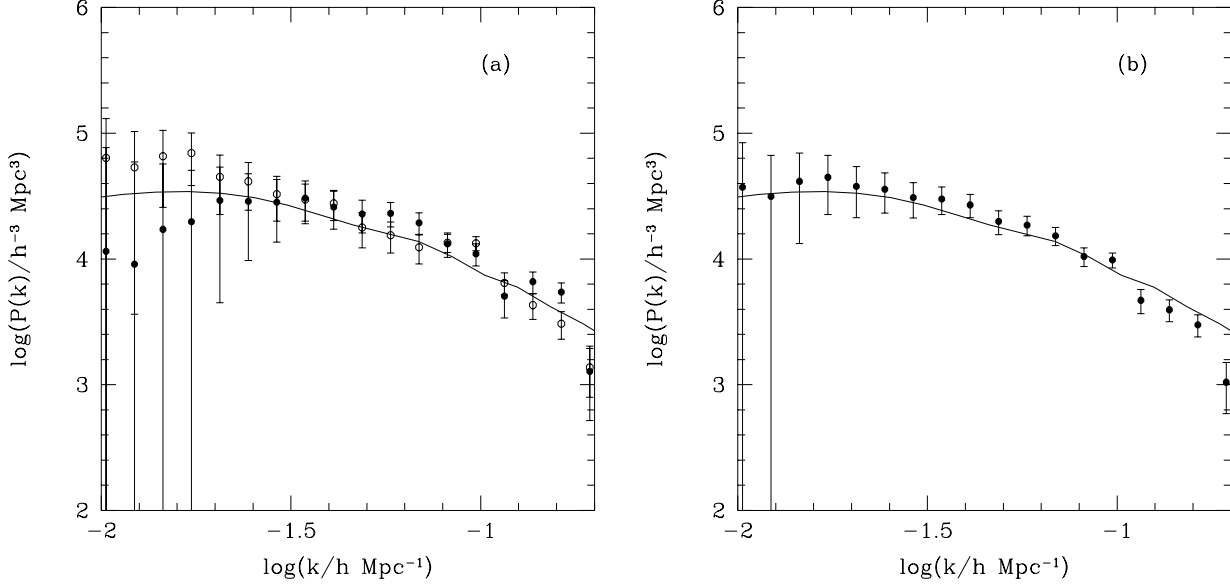


Figure 6. The points in the left hand plot show the power spectra measure from mock SGC simulations (open circles) and mock NGC simulations (closed circles). These are combined in the right hand plot, as described in the text, to give a single mock power spectrum with the current angular selection function imprinted on the mock catalogues. The solid line in both plots is the input power spectrum, as described in Figure 5. The power spectrum measured with the current angular selection function imprinted matches the input power spectrum over a wide range of scales. In both plots, the errors are FKP errors and we use a FFT to measure the power spectra on scales larger than $70h^{-1}\text{Mpc}$ ($\log(k/h\text{Mpc}^{-1})=-1.12$) and the direct method on smaller scales. The simulation has the Λ cosmology.

tra for the two choices of cosmology. We measure the power spectrum from QSOs with redshifts in the range $0.3 < z < 2.2$ where the photometric completeness is higher than ≈ 90 per cent Boyle (2000) and the number density remains approximately constant.

In Figure 7 we compare the NGC and SGC power spectra measured from QSOs with redshift in the range $0.3 < z < 2.2$ assuming the EdS cosmology (a) and the Λ cosmology (b). The combined power spectra are shown in (c, EdS cosmology) and (d, Λ cosmology). There is good agreement between the power spectrum measured from the NGC and the SGC strips over a wide range of scales. The errors we show here and through out are 1σ errors.

The power spectra have a power-law form with $P_{\text{QSO}}(k) \propto k^\alpha$ with $\alpha \sim -1.3$ for both choices of cosmology (-1.26 ± 0.15 EdS and -1.31 ± 0.16 Λ) over the range $-1.7 < \log(k) < -1$ ($60\text{-}300h^{-1}\text{Mpc}$).

CDM models predict that the power spectrum should turn over at a scale which depends on the shape parameter, Γ , of the power spectrum. In pure CDM models with a scale-invariant spectrum of initial fluctuations $\Gamma = \Omega_m * h$. This relation becomes more complicated, however, with the addition of baryons, hot dark matter, or a tilted initial fluctuations spectrum, and so a measurement of Gamma cannot be reliably inverted to imply a measurement of $\Omega_m * h$ (Sugiyama 1995, Peacock 2000). If $\Gamma > 0.25$ then the turnover should occur on scales less than $300h^{-1}\text{Mpc}$. The fact that we do not see a turnover puts constraints on the range of acceptable Γ values. In Section 6, we compare the data to models to constrain the value of Γ further.

We tentatively identify a ‘spike’ feature at $\log(k/h\text{Mpc}^{-1}) \approx -1.16$ ($90 h^{-1}\text{Mpc}$) assuming the Λ cosmology and at $\log(k/h\text{Mpc}^{-1}) \approx -1.01$ ($65 h^{-1}\text{Mpc}$) as-

suming the EdS. Figures 7(a,b) show that the feature seems to reproduce in the NGC and SGC strips. We shall see in Figure 9(a,b) that this feature also appears to reproduce in the two independent redshift bins in both cosmologies. In both cases, the spike feature lies about 2σ above the power-law fit to the power spectrum. (slightly higher in the Λ case, slightly lower in the EdS case), corresponding to a probability of 1/20 that a point deviates from the fit, neglecting the fact that the points may not be completely independent. With 17 data points, we should expect one point to deviate by this amount so the spike feature is marginal. However, if real, such a feature might be caused by acoustic oscillations in the baryon-radiation fluid prior to decoupling. If this power spectrum spike is confirmed in the analysis of the full 2QZ, it would also provide a powerful measure of the world model. Such features do not evolve in scale as a function of redshift and a comparison between the 2QZ $P(k)$, measured at a mean redshift of 1.4 and the galaxy $P(k)$ measured at $z \approx 0$ may allow constraints on Ω_m and Ω_Λ via the requirement to maintain the feature at the same scale in both power spectra. For example, preliminary reports of results from the 2dF Galaxy Redshift Survey power spectrum (Peacock et al. 2001) show some possible indications of a spike detected in their data at $\log(k/h\text{Mpc}^{-1}) \approx -1.12$ ($85h^{-1}\text{Mpc}$), assuming the Λ cosmology, although the 2dFGRS team do not claim that any single isolated feature in their data is significant. In an EdS cosmology this feature would lie at $\log(k/h\text{Mpc}^{-1}) \approx -1.08$ ($75h^{-1}\text{Mpc}$). The low redshift galaxy result may therefore be somewhat more consistent with the high redshift QSO result assuming the Λ cosmology but more QSO and galaxy data will clearly be needed at both high and low redshift before a final conclusion can be drawn.

We have used the CMBFAST programme (Seljak & Zal-

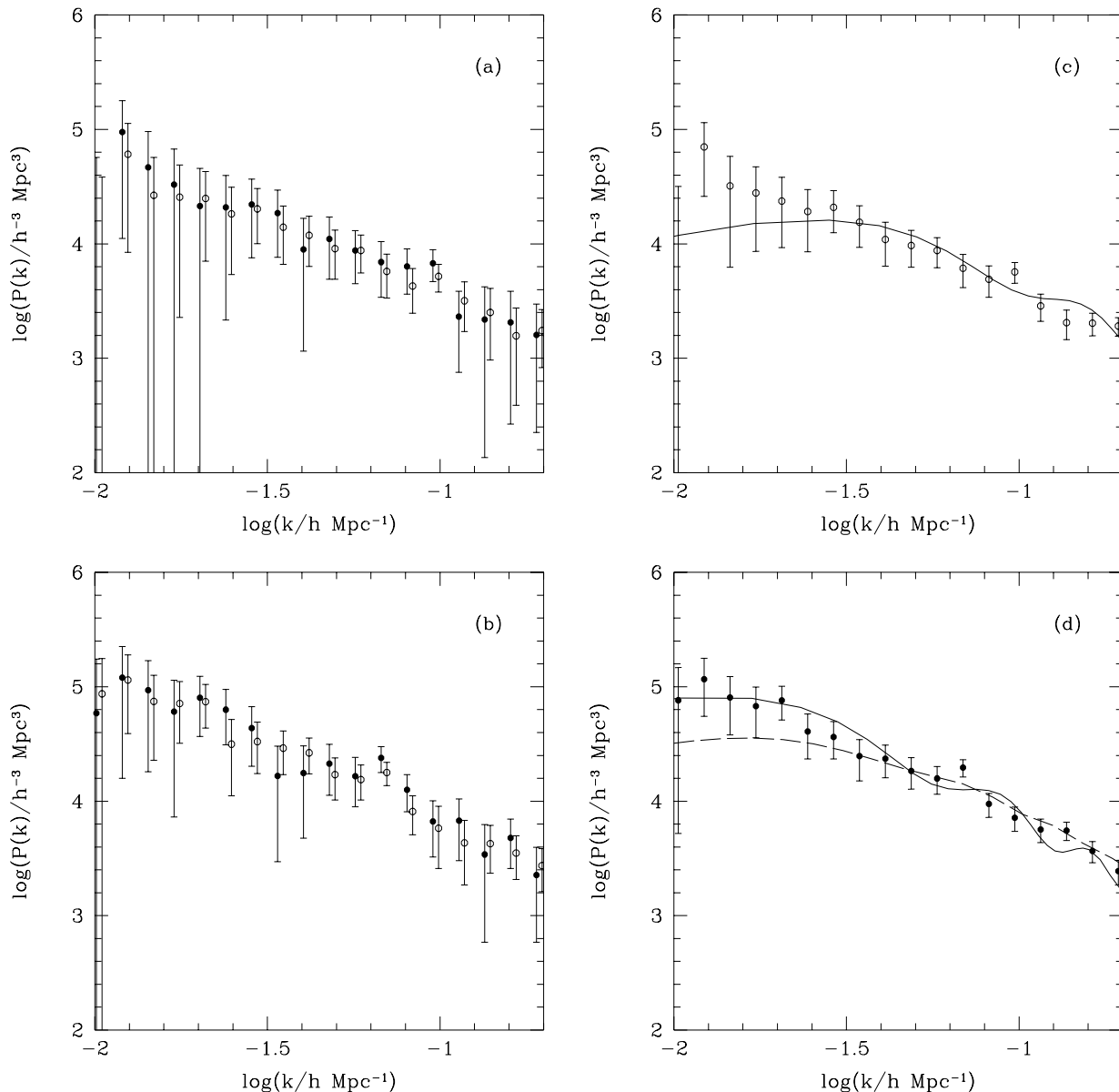


Figure 7. In Figures (a) and (b) we compare the power spectrum from the NGC (filled circles) and SGC (open circles). Both sets of points have been offset by 0.01 in $\log(k/h \text{ Mpc}^{-1})$ for clarity. In Figures (c) and (d) we show the combined QSO power spectra. The EdS cosmology is assumed for (a) and (c) and the Λ cosmology for (b) and (d). The solid lines in (c, d) show models with an increased baryon fraction (described in the text) to try and reproduce the feature present in the QSO power spectra. The dashed line in (d) is the input power spectrum to the *Hubble Volume* simulation. QSOs have redshifts in the range $0.3 < z < 2.2$.

darriaga 1996) to see how close the feature might be in scale and amplitude to the second baryon-radiation acoustic peak. Generally, for a wide range of Ω_b and h in both the EdS and the Λ cosmology, the peak scale appears at $\gtrsim 25$ per cent smaller wavenumber than the predicted second peak. Also the amplitude of the peak appears to demand a higher value of Ω_b than used in e.g. the Λ CDM *Hubble Volume* model ($\Omega_\Lambda=0.7$, $\Omega_m=0.3$, $\Omega_b=0.04$, $h=0.7$). To illustrate this, the *Hubble Volume* input spectrum is shown in Figure 7(d) together with a CMBFAST prediction with $\Omega_\Lambda=0.7$, $\Omega_m=0.3$, $\Omega_b=0.1$, $h=0.5$. This model gives as good a fit as any to the observed spike feature but, although having a reasonable amplitude, it lies at $\log(k/h \text{ Mpc}^{-1})=-1.05$ rather than the

observed $\log(k/h \text{ Mpc}^{-1})=-1.16$. Figure 7(c) shows a CMBFAST model with $\Omega_m=1$, $\Omega_b=0.3$, $h=0.3$ again as an example of a model which gets as close as any to matching the observed feature. However, again the predicted spike lies at too large a wavenumber, $\log(k/h \text{ Mpc}^{-1})=-0.82$, compared to the observed spike scale of $\log(k/h \text{ Mpc}^{-1})=-1.02$. We also note that Meiksin, White & Peacock (1999) have suggested that quasi-linear evolution may reduce the predicted amplitude of the second acoustic peak. We postpone further discussion of the theoretical implications of the spike feature until we see if it reproduces in our full 25k 2QZ sample.

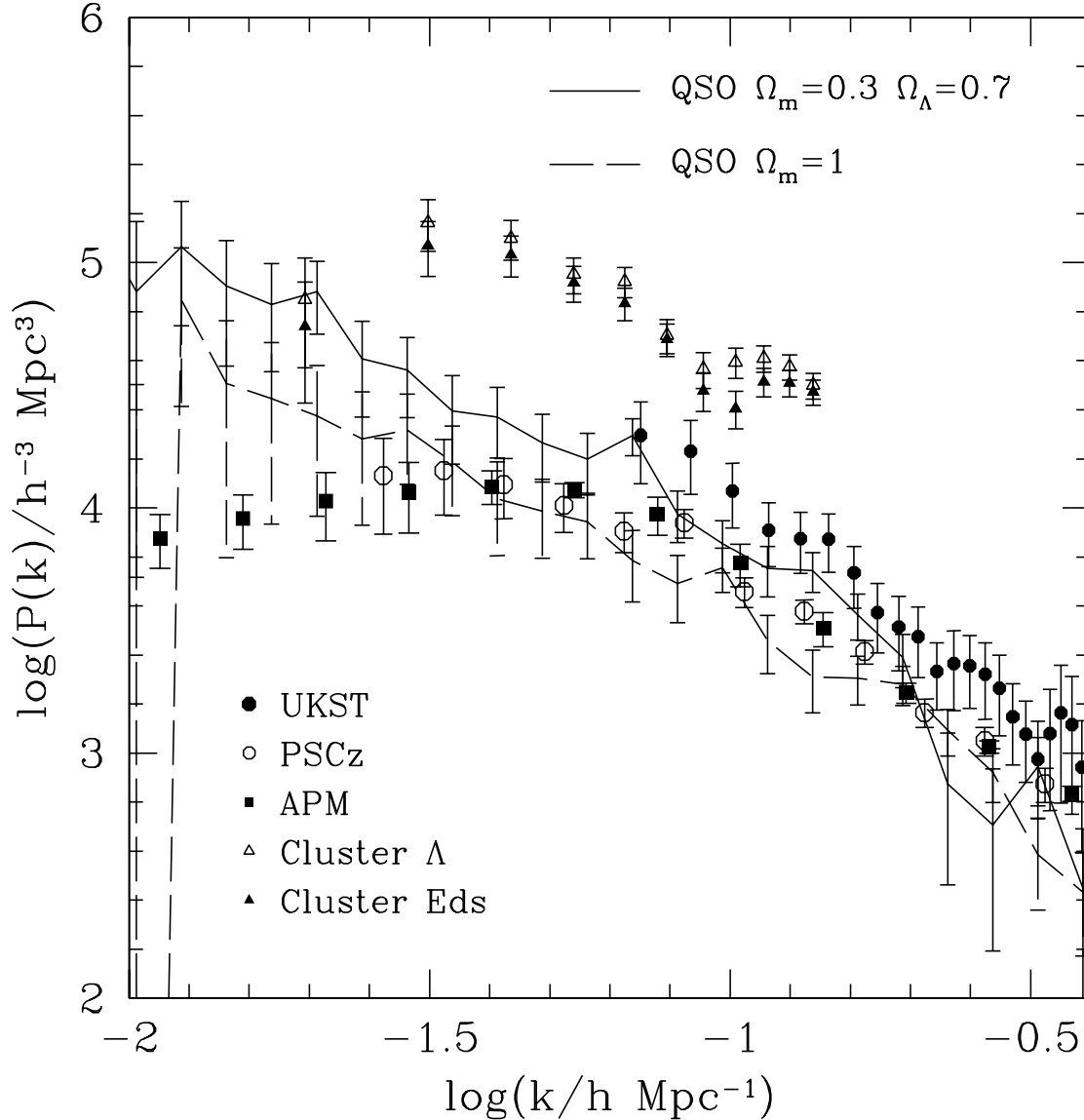


Figure 8. A comparison of galaxy and QSO power spectra. The lines show the QSO power spectra with the Λ cosmology (solid line) and the EdS cosmology (dashed line) assumed. The filled circles show a flux limited power spectrum measured from the Durham/UKST Survey (Hoyle et al. 1999), the open circles show the power spectrum measured from the PSCz Survey (Sutherland et al. 1999). The filled squares show the APM real space galaxy power spectrum taken from Baugh & Efstathiou (1994). The triangles show the power spectrum of rich clusters with $\Omega_m=1$ (filled) and $\Omega_m=0.2$, $\Omega_\Lambda=0.8$ (open) taken from Tadros, Efstathiou & Dalton (1998). The errors on the QSO power spectra are 1σ FKP errors, the errors on the Durham/UKST and PSCz galaxy power spectrum and the errors on the cluster power spectrum are from mock catalogues. The errors on the APM power spectrum are obtained by measuring the scatter in power spectra obtained from four separate regions of the APM survey.

5.2 Comparison with $P(k)$ from Galaxy and Cluster Surveys

The power spectrum of optically selected galaxies has been measured from several different galaxy surveys but so far only out to $\approx 100h^{-1}\text{Mpc}$ scales. In Figure 8, we compare the power spectrum estimated from the QSOs currently observed in 2QZ, assuming two different cosmologies, with a power spectrum from the Durham/UKST survey (Hoyle et al. 1999). The lines show the QSO power spectrum, estimated assuming the Λ cosmology (solid line) and the EdS

cosmology (dashed line). The filled circles show a flux limited galaxy power spectrum with $P=8000h^{-3}\text{Mpc}^3$ fixed in the weighting scheme of Feldman, Kaiser & Peacock (1994).

Figure 8 shows that the form of the QSO and galaxy redshift space power spectra are similar, although the range of overlap where the two power spectra are robustly measured is small. The slopes are statistically consistent whether the QSO power spectrum is computed in the EdS or Λ cosmology. In the final sample there may be a possible cosmological test afforded by comparing the slopes of QSO power

spectra with power spectra obtained at lower redshift, if the bias can be assumed to be scale independent. The QSO power spectrum in the Λ case has a amplitude slightly lower than that of the galaxy power spectra. If an EdS cosmology is assumed, the amplitude of the QSO power spectrum (dashed line) is approximately a factor of ≈ 3 lower than the galaxy power spectra. Croom et al. (2001) found very similar results in the comparison of galaxy and QSO clustering amplitudes in their correlation function analysis of the 2QZ data.

We compare the QSO power spectra to the PSCz Survey power spectrum (Sutherland et al. 1999) in Figure 8. The PSCz Survey is an Infra-Red selected redshift survey. Comparisons between optically and IR selected surveys reveal that there is typically an offset between clustering statistics between the two surveys with $P_{\text{Opt}} = 1.3^2 P_{\text{IR}}$ (Hoyle et al. 1999) which explains why the PSCz $P(k)$ has an amplitude that is in closer agreement with the EdS QSO $P(k)$ than the Λ $P(k)$, contrary to the optical comparison.

We also compare the QSO power spectra to the real space APM galaxy power spectrum of Baugh & Efstathiou (1994), inferred from measurements of the angular correlation function, $w(\theta)$. The real space APM galaxy power spectrum has a lower amplitude than the Durham/UKST redshift space power spectrum as bulk motions of galaxies increase amplitude of the redshift space power spectrum (Kaiser 1987). There is also some uncertainty in the normalisation of the APM power spectrum due to the inversion technique of estimating the power spectrum (Carlton Baugh, private communication). On scales out to $100 h^{-1} \text{Mpc}$ ($\log(k/h \text{Mpc}^{-1}) = -1.2$), there is reasonable agreement between the amplitudes of the different power spectra. On scales larger than $100 h^{-1} \text{Mpc}$, the APM power spectrum flattens off, whereas the QSO power spectra continue to rise. We believe that the QSO power spectra measurements are robust to $300 h^{-1} \text{Mpc}$ assuming the EdS cosmology ($400 h^{-1} \text{Mpc}$ assuming the Λ cosmology). Therefore we find even more large scale power than in the APM power spectrum and possibly even more power than the Λ CDM models (see Section 6).

A final comparison is made between the QSO power spectra and the power spectra of rich clusters of galaxies. In Figure 8, the triangles show the APM Cluster Survey power spectra taken from Tadros, Efstathiou & Dalton (1998). The cluster power spectra are found assuming $\Omega_m=1$ (filled triangles) and $\Omega_m=0.2$, $\Omega_\Lambda=0.8$ (open triangles). As the clusters are only observed out to a redshift of ≈ 0.2 , the effects of cosmology on the clustering amplitude are small so the two cluster power spectra have a similar amplitude and shape. The slopes of the QSO power spectra are similar to those for the clusters for both models, within the overlapping range of scales. As can clearly be seen in Figure 8, the QSOs have a lower clustering amplitude than the present day rich clusters. We shall see below that the QSO power spectrum amplitude only evolves slowly with redshift and so it is meaningful to compare the QSO and cluster power spectra. The relative bias between the two types of power spectra is $b_{\text{rel}} \approx \sqrt{5}$ for the Λ cosmology and $b_{\text{rel}} \approx \sqrt{10}$ for the EdS cosmology.

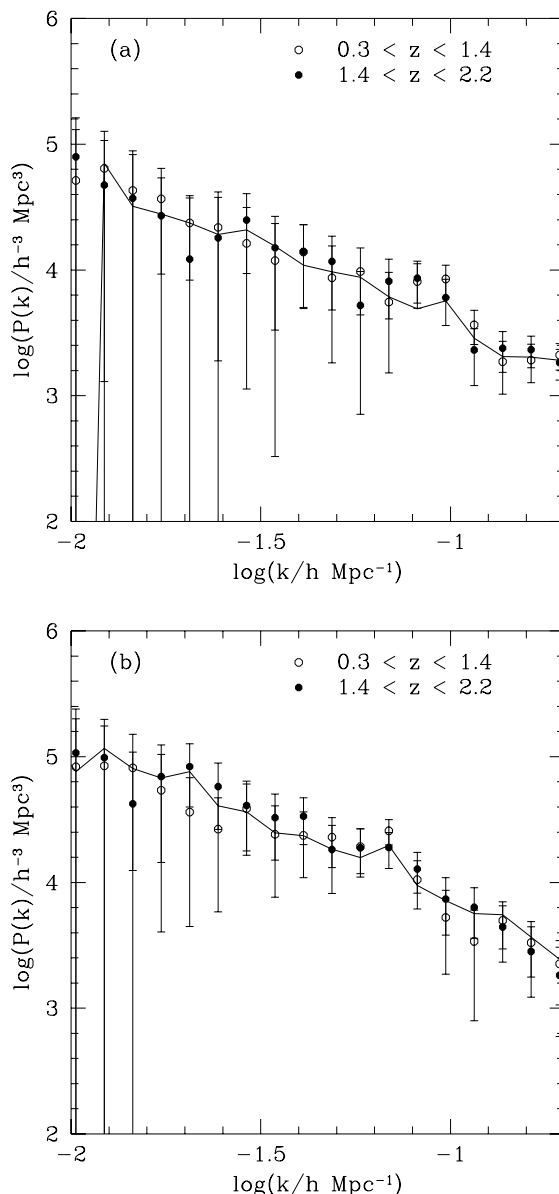


Figure 9. The power spectrum of QSOs measured at different redshifts. The EdS cosmology is assumed in (a) and the Λ cosmology is assumed in (b). In both panels, the solid line shows the power spectrum estimated from all the QSOs with $0.3 < z < 2.2$, as in Figure 10. The open circles show the power spectrum of QSOs with redshifts in the range $0.3 < z < 1.4$ and the filled circles show the power spectrum of QSOs with redshifts in the range $1.4 < z < 2.2$. The errors are 1σ FKP errors. The points are slightly offset for clarity.

5.3 The Evolution of QSO Clustering

To determine how QSO clustering evolves as a function of redshift, we split the QSOs in each strip of the survey into two redshift bins containing roughly equal numbers of QSOs, one with QSOs in the range $0.3 < z < 1.4$ ($\bar{z} = 1.0$) and the other with $1.4 < z < 2.4$ ($\bar{z} = 1.8$). The power spectrum is then measured from each subsample on each strip, assuming the two cosmologies discussed in Section 2. The results from the NGC and SGC for each redshift bin and for each

cosmology are averaged together as before. All the power spectra in Figure 9(a) are estimated assuming the EdS cosmology, whilst in panel (b), the Λ cosmology is assumed. In both panels, the solid line shows the power spectrum of all the QSOs, the open circles show the power spectrum of the low redshift QSOs and the filled circles show the power spectrum of the high redshift QSOs.

When the QSOs are split up into the two samples, the errors on the measured power spectra are increased. However, on scales around $100\text{--}200h^{-1}\text{Mpc}$ ($-1.2 > \log(k/h\text{Mpc}^{-1}) > -1.5$) the power spectrum can still be fairly well measured, the fractional errors are around 40 per cent. There is reasonable agreement between the power spectra measured from the two redshift bins over a wide range of scales. In order to compare the amplitudes of high and low redshift power spectra, we assume that they are both power laws of the form $\log(P/h^{-3}\text{Mpc}^3) = \alpha\log(k/h\text{Mpc}^{-1}) + A$. We fix α to be -1.3 and find the best fitting value of the amplitude, A , over the range $-1.6 < \log(k/h\text{Mpc}^{-1}) < -1.2$ in the case of the Λ cosmology and $-1.5 < \log(k/h\text{Mpc}^{-1}) < -1.1$ for the EdS case (corresponding to scales of $100\text{--}250h^{-1}\text{Mpc}$ for the Λ case and $75\text{--}200h^{-1}\text{Mpc}$ in the EdS case). In the Λ cosmology, the high redshift bin has an amplitude of 2.58 ± 0.09 and the low redshift bin has an amplitude of 2.63 ± 0.08 . In the EdS case, the high redshift bin has an amplitude of 2.31 ± 0.09 and the low amplitude bin has an amplitude of 2.29 ± 0.10 . This shows that QSO clustering does not evolve strongly with redshift as the low and high redshift bins have power law fits that are consistent in amplitude.

This result is consistent with the work of Croom et al. (2001) who have measured the clustering from the 10k QSO catalogue in five bins of redshift. If the EdS cosmology is assumed then little evolution is seen in the clustering amplitude of QSOs, consistent with Croom & Shanks (1996). If the Λ cosmology is assumed, slow evolution is seen in the clustering amplitude of QSOs, with QSOs at high redshift having a slightly higher clustering amplitude than QSOs at low redshift.

The slow evolution in QSO clustering was interpreted previously in terms of cosmology and the effects of QSO bias (see, for example, Croom & Shanks 1996). The slow evolution either suggests that Ω_m is low, less than 0.1, so that the dark matter clustering does not evolve strongly with redshift, or if Ω_m is fairly high, $\gtrsim 0.1$, then bias evolves as a function of redshift to counteract the decrease in amplitude of the dark matter clustering. Croom et al. (2001) make a detailed comparison between the evolution of QSO clustering and various models for the QSO-mass bias. Determining cosmology from the evolution of QSO clustering alone is not possible due to the degeneracy between cosmology and bias.

Since the QSO power spectra have comparable amplitudes to local galaxy power spectra and since the slow QSO clustering evolution implies that the QSO amplitude does not increase markedly at low redshift, this suggests that QSOs are not highly biased objects with respect to present day optically selected galaxies.

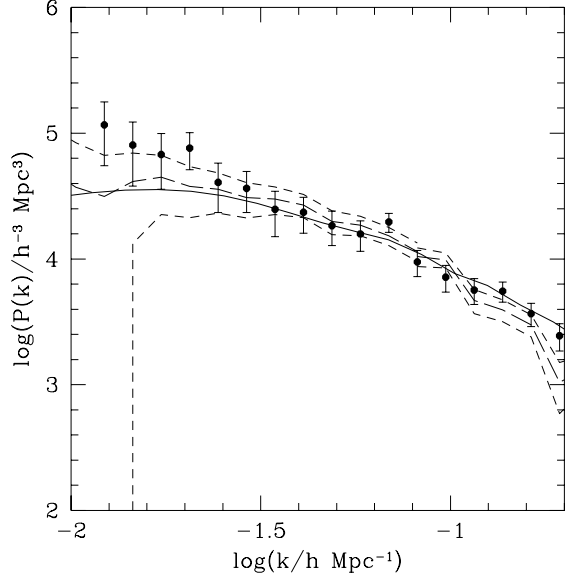


Figure 10. The points show the power spectrum from the 10k QSO catalogue with the Λ cosmology assumed. The solid line shows the real space input power spectra to the *Hubble Volume* simulation. The dashed lines show the mock catalogue redshift space power spectrum and errors from Figure 6(b), discussed in the text.

6 COMPARISON WITH MODELS OF LARGE SCALE STRUCTURE

As discussed previously, it is the power spectrum of the mass density field that is predicted by models of large scale structure. If the bias between the dark matter and QSOs can be written as $P(k)_{\text{QSO}} = b^2 P(k)_{\text{mass}}$, with b a constant, which could be the case on large scales (Coles 1993; Cole et al 1998; Mann, Peacock & Heavens 1998), it is meaningful to compare the shapes of mass and QSO power spectra.

However, we find that the current incompleteness may be introducing a slight bias into the shape of the QSO power spectrum. The shape of the power spectrum from the mock catalogues with the incompleteness imprinted on them is slightly steeper than the input power spectrum to the simulation. This is shown in Figure 10. The solid line shows the input power spectrum, the long dashed line shows the power spectrum from the mock catalogues with the current angular selection function imprinted on them (as seen in Figure 6(b), the short dashed lines are the 1σ errors). The points show the QSO power spectrum calculated assuming the Λ cosmology. On the smallest scales, the dashed line is inconsistent with the solid line at the 1σ level, although on these small scales the FKP errors may underestimate the true error. Therefore, we fit the model power spectra to the QSO power spectrum, assuming the Λ cosmology, down to $60h^{-1}\text{Mpc}$ ($\log(k/h\text{Mpc}^{-1}) = -1$). We have no mock catalogues with the EdS cosmology to test if incompleteness affects the shape of the QSO power spectrum from the 10k QSO catalogue, assuming the EdS cosmology. However, we wish to fit the models to the data over the same range of $\log(k/h\text{Mpc}^{-1})$ so we fix the lower limit for the EdS case to be $\log(k/h\text{Mpc}^{-1}) = -0.9$ ($50h^{-1}\text{Mpc}$). We set the limit on large scales to be the scale where the geometry of the

survey affects the shape of the power spectrum. This corresponds to $300h^{-1}\text{Mpc}$ ($\log(k/h\text{Mpc}^{-1})=-1.7$) in the EdS cosmology and $400h^{-1}\text{Mpc}$ ($\log(k/h\text{Mpc}^{-1})=-1.8$) in the Λ cosmology.

We compare the QSO power spectra to model CDM power spectra with different values of the shape parameter Γ , introduced in Section 5.1. We assume the fit to the CDM transfer function given by Bardeen et al. (1986). The power spectrum is calculated at $z = 1.4$ rather than at $z = 0$ to approximate the dark matter power spectrum averaged over the lightcone. We assume a value of σ_8 that matches the cluster normalisation for each cosmology given by Eke, Cole & Frenk (1996). For each cosmology, the model power spectra are χ^2 fitted to the QSO power spectrum to find the factor, b_{eff} , required to match the two as well as possible.

We choose values of Γ in the range $0.05 < \Gamma < 0.5$ which more than covers the range of values that fit current galaxy power spectra, such as the APM real space power spectrum (Eisenstein & Zaldarriaga 2001). We note that ΛCDM models with $\Gamma \gtrsim 0.3$ are not physically motivated but we are just comparing a range of models with different shapes to the QSO power spectrum and we do indeed find that models with values of $\Gamma \gtrsim 0.3$ give a poor fit to the QSO power spectrum with the Λ cosmology assumed.

In Figure 11, we show the QSO power spectrum with the EdS cosmology (open circles, a) and with the Λ cosmology (solid circles, b). The lines have different values of Γ : $\Gamma=0.5$ (solid), $\Gamma=0.4$ (short - long dashed), $\Gamma=0.3$ (short dashed), $\Gamma=0.2$ (long dashed) and $\Gamma=0.1$ (dotted). Models with $\Gamma=0.5$ are ruled out at more than 3σ assuming either cosmology. This is in agreement with results from galaxy surveys. More large scale power was found in the galaxy correlation function from the APM Survey than expected from the standard CDM $\Gamma=0.5$ model (Efstathiou, Sutherland & Maddox 1990). This led to variants of the CDM model, such as ΛCDM and τCDM to be developed.

In both cases, the best agreement between the models and the QSO power spectra is found with a model with low values of Γ . Models with $\Gamma=0.12 \pm 0.10$ best fit the shape of the QSO power spectrum assuming the EdS cosmology and models with lower values of $\Gamma = 0.11 \pm 0.1$ best fit the QSO power spectrum assuming the Λ cosmology. The input power spectrum to the ΛCDM *Hubble Volume* has a shape of $\Gamma=0.17$. This model is therefore consistent with the data at the 1σ level.

The results found here are in reasonable agreement with those of Croom et al. (2001). They find that models with $\Gamma=0.5$ do not provide a good fit to the correlation function measured from the 10k QSO catalogue assuming the EdS and the Λ cosmology. Models with $\Gamma=0.1-0.2$ are required to fit the correlation function with the Λ cosmology assumed. However, models with $\Gamma=0.2-0.4$ best fit the correlation function if the EdS cosmology is assumed.

This test is quite simplistic as possible effects of the incompleteness have not been included in the shape of the model power spectrum, although by fitting to a limited range of scales we should have reduced the effect that this can have on the models that fit the power spectrum. When 2QZ is finished, we will be able to compare the models over a wider range of scales and produce stronger constraints on the range of acceptable Γ parameters.

In order to thoroughly test models of structure forma-

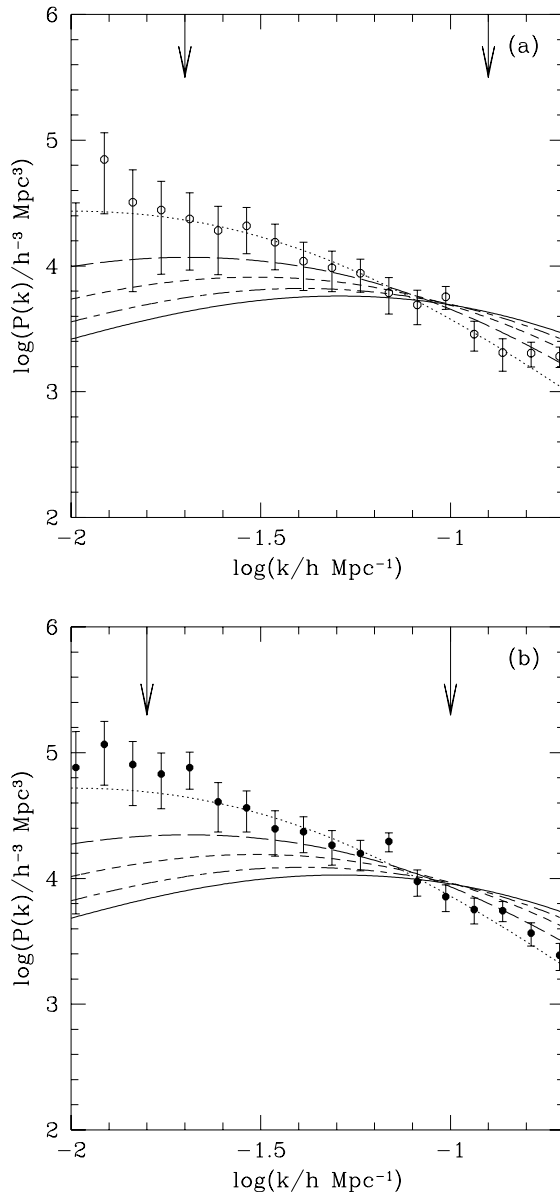


Figure 11. Comparison of different model power spectra to the QSO power spectra for the two choices of cosmology. The solid circles in panel (a) show the QSO $P(k)$ with the Λ cosmology assumed and the open circles in panel (b) show the QSO $P(k)$ with the EdS cosmology assumed. In both panels the matching lines show the same Γ values with $\Gamma=0.5$ (solid line), 0.4 (short - long dashed), 0.3 (short dashed), 0.2 (long dashed) and 0.1 (dotted). Each line is plotted at the amplitude that gives the best fit to the QSO power spectrum. The arrows indicate the range of scales over which the fit was made.

tion, full N-body simulations, such as the *Hubble Volume* are required. However, due to the large volume of 2QZ, large amounts of super-computing time are required to carry out such simulations so it is currently not possible to run them for a wide range of cosmological models. Physically motivated models for selecting QSOs within the simulation are also required as a linear bias between the mass and the QSOs may be an over simplification, even on these large scales.

7 DISCUSSION AND CONCLUSIONS

We have presented the first QSO power spectrum analysis using the 10k catalogue from the 2dF QSO Redshift Survey. The QSO power spectrum has a power law form with $P_{\text{QSO}}(k) \propto k^{-1.3 \pm 0.15}$ which appears to extend to large scales. More large scale power is seen in the QSO power spectra than in the APM power galaxy spectrum even.

The clustering environment observed for radio-quiet QSOs in CCD imaging experiments is close to that of optically selected galaxies, (Ellingson, Yee & Green 1991; Smith, Boyle & Maddox 1995, 1999; Croom & Shanks 1999) suggesting that the biasing of QSOs may be no stronger than it is for galaxies; at the $r > 50h^{-1}\text{Mpc}$ scales considered here the assumption that the QSO-mass bias is scale independent may therefore be reasonable. Therefore, the fact that we do not see a turnover on scales up to $300h^{-1}\text{Mpc}$ places a strong constraint on the value of the shape parameter, requiring $\Gamma \lesssim 0.25$. We find that the large scale power seen in the QSO power spectrum is best fit by Λ CDM models with Γ as low as 0.1 ± 0.1 .

A power spectrum analysis of mock QSO catalogues, created from the Virgo Consortium's Hubble Volume Λ CDM simulation, with $\Gamma = 0.17$ as input, produces a result which is statistically consistent with the data. The analysis of the mock catalogues indicates that we are able to produce a first robust measurement of the QSO power spectrum over a wide range of scales and thus the above results for Γ are unlikely to be dominated by systematic effects due to the current incompleteness of the 2QZ catalogue.

We note that the low Γ values measured here from the shapes of the QSO power spectra are in some disagreement with the best fit parameters as measured from the Boomerang and MAXIMA CMB power spectra (Balbi 2000, de Bernadis 2000). Bond et al. (2000) measures $\Omega_b h^2 = 0.03$ and $\Omega_{\text{CDM}} h^2 = 0.17$ for $\Omega_m h^2 = 0.2$ in a spatially flat model. For $h = 0.65$ this implies $\Gamma = \Omega_m h = 0.3$ which is rejected at 2σ in Figures 11(a, b). It will be interesting to see if this discrepancy persists as more CMB and 2QZ data accumulate.

We measure the QSO power spectrum in two bins of redshift and find that the clustering can only evolve slowly as a function of redshift as QSOs with a median redshift of $\bar{z} = 1.0$ have a clustering amplitude consistent with that of QSOs with a median redshift of $\bar{z} = 1.8$. This is consistent with the results of Croom et al. (2001), who find little evolution in the amplitude of QSO clustering as a function of redshift if the EdS cosmology is assumed and only slow evolution if a Λ cosmology is assumed.

The QSO power spectrum, which is therefore broadly independent of redshift, lies close in amplitude to the power spectrum of local, optically selected galaxies. The range of scales where the two overlap is limited, but once the 2dF Galaxy Redshift Survey is finished, an interesting comparison between power spectra of optically selected QSOs and galaxies over a wide range of scales will be possible. The power spectrum of rich galaxy clusters measured by Tadros, Efstathiou & Dalton (1998) has a far higher clustering amplitude than the QSO power spectrum, again suggesting that the QSO-mass bias is much closer to galaxies than galaxy clusters.

We tentatively detect a 'spike' feature at $\approx 90h^{-1}\text{Mpc}$ assuming the Λ cosmology or $\approx 65h^{-1}\text{Mpc}$ assuming the

EdS cosmology. This feature appears to reproduce in both the NGC and SGC strips and in independent redshift bins but its statistical significance is still marginal. An investigation using CMBFAST indicates that the spike is seen at a $\gtrsim 25$ per cent smaller wavenumber than the second peak caused by acoustic oscillation in the pre-recombination baryon-radiation fluid. Somewhat higher values of Ω_b than usually assumed in Λ CDM models may also be needed to fit the amplitude of the feature. It will be interesting to see if this feature persists in the final 25k 2QZ survey $P(k)$. Since it lies well into the linear regime where it will evolve little with redshift under the correct assumed cosmology it could therefore act as an important probe of world models.

The QSO power spectrum is currently measured to an accuracy of $\lesssim 30\%$ over the range of scales $60 \lesssim r \lesssim 200h^{-1}\text{Mpc}$ for either the EdS or Λ cosmology adopted here. On these scales, we predict the errors will be approximately 1.5 times smaller in the completed 2QZ catalogue. The power spectrum from the 25k catalogue will also be measurable out to scales of $\lesssim 600h^{-1}\text{Mpc}$. Thus, when these data become available, there is the promise of placing even stronger constraints on the large scale structure of the Universe and hence on the underlying cosmological model.

ACKNOWLEDGMENTS

We would like to recognise the considerable efforts of all the AAT staff responsible for the operation of the 2dF instrument which has made this survey possible. We would also thank our colleagues on the 2dF galaxy redshift survey team, in particular Gavin Dalton and Steve Maddox, for facilitating many of the survey observations and John Peacock and Shaun Cole for useful comments. We also thank the Virgo Consortium, especially Adrian Jenkins and Gus Evrard, for providing the *Hubble Volume* simulations. FH and NL acknowledge the receipt of a PPARC studentship.

REFERENCES

- Bailey J. & Glazebrook K., 1999, 2dF User Manual, Anglo Australian Observatory
- Balbi A. et al., 2000, ApJ, 454, 1
- Bardeen J. M., Bond J. R., Kaiser N. & Szalay A., 1986, ApJ, 304, 15
- Baugh C.M. & Efstathiou G., 1993, MNRAS, 265, 145
- Baugh C.M. & Efstathiou G., 1994, MNRAS, 270, 183
- Bond J. R. et al., 2000, astro-ph/0011378
- Boyle B. J., 1986, PhD Thesis, University of Durham
- Boyle B. J., Shanks T., Croom S. M., Smith R. J., Miller L., Loaring N. & Heymans C., 2000, MNRAS, 317, 1014
- Cole S. M., Fisher K. B. & Weinberg D. H., 1995, MNRAS, 267, 785
- Cole S. M., Hatton S. J., Weinberg D. H. & Frenk C. S., 1998, MNRAS, 300, 945
- Coles P., 1993, MNRAS, 262, 1065.
- Colless M., 1998, 'Looking Deep in the Southern Sky', eds Morganti R. & Couch W. J., ESO/Australia Workshop, Springer, Pg 9
- Crampton D., Le Fèvre O., Lilly S. J. & Hammer F., 1995, ApJ, 455, 96
- Croft R. A. C., Weinberg D. H., Katz N. & Hernquist L., 1998, ApJ, 495, 44

- Croom S. M., 1997, PhD Thesis, University of Durham
- Croom S. M. & Shanks T., 1996, MNRAS, 281, 893
- Croom S. M. & Shanks T., 1999, MNRAS, 303, 411
- Croom S. M., Shanks T., Boyle B. J., Smith R. J., Miller L. & Loaring N., 1998, Evolution of Large Scale Structure: From Recombination to Garching
- Croom S. M., Shanks T., Boyle B. J., Smith R. J., Miller L., Loaring N. S. & Hoyle F., 2001, MNRAS, 325, 483
- de Bernardis P. et al., 2000, Nature, 404, 955
- Davis M. & Faber S. M., 1998, in 'Wide Field Surveys in Cosmology', Editions Frontieres, ISBN 2-8 6332-241-9, 333
- Efstathiou G., Sutherland W. J. & Maddox S. J., 1990, Nature, 348, 705
- Eisenstein D. J. & Zaldarriaga M., 2001, ApJ, 546, 2
- Eke V. R., Cole S. M. & Frenk C. S., 1996, MNRAS, 282, 263
- Ellingson E., Yee H. K. C. & Green R.F., 1991, ApJ, 371, 49
- Feldman H. A., Kaiser N. & Peacock J. A., 1994, ApJ, 426, 23
- Frenk C.S. et al., 2000, astro-ph/0007362
- Gunn J. E. & Weinberg D. H., 1995, in proceedings of the 35th Herstmonceux workshop, Cambridge University Press, Cambridge
- Hatton S. J., 1999, PhD Thesis, University of Durham
- Hewitt P. C., Foltz C. B. & Chaffee F. H., 1995, AJ, 109, 1498
- Hoyle F., 2000, PhD Thesis, University of Durham
- Hoyle F., Baugh C. M., Shanks T. & Ratcliffe A., 1999, MNRAS, 309, 659
- Kaiser N., 1987, MNRAS, 227, 1
- La Franca F., Andreani P. & Cristiani S., 1998, ApJ, 497, 529
- Le Fèvre O. et al., 1998, in 'Wide Field Surveys in Cosmology', Editions Frontieres, ISBN 2-8 6332-241-9, 333
- Lin H., Kirschner P., Shectman S. A., Landy S. D., Oemler A., Tucker D. L. & Schechter P. L., 1996, ApJ, 471, 617
- Mann R. G., Peacock J. A. & Heavens A. F., 1998, MNRAS, 293, 209.
- Meiksin A. & White M., 1999, MNRAS, 308, 1179
- Meiksin A., White M. & Peacock J. A., 1999, MNRAS, 304, 851
- Miller L., et al., 2001, in preparation
- Osmer P. S., 1981, ApJ, 247, 762
- Peacock J. A., 2000, astro-ph/0002013
- Peacock J. A. et al., 2001, in Proceedings of the 20th Texas Symposium on Relativistic Astrophysics
- Schlegel D. J., Finkbeiner D. P. & Davis M., 1998, ApJ, 500, 525
- Seljak U. & Zaldarriaga M., 1996, ApJ, 469, 437
- Shanks T., Fong R., Boyle B. J. & Peterson B. A., 1986, In IAU Symp No 119 on Quasars, eds Swarup G. & Kapahi V. K., Reidel, Dordrecht, Holland
- Shanks T., Fong R., Boyle B. J. & Peterson B. A., 1987, MNRAS, 271, 753
- Shaver P. A., 1984, A&A, 136, L9
- Smith R. J., 1998, PhD Thesis, University of Cambridge
- Smith R. J., Boyle B. J. & Maddox S. J., 1995, MNRAS, 277, 270
- Smith R. J., Boyle B. J. & Maddox S. J., 2000, MNRAS, 313, 252
- Smith R. J., Croom S. M., Boyle B. J., Shanks T., Miller L. & Loaring N. S., 2001, MNRAS submitted
- Steidel C. C., Adelberger K. L., Gialisco M., Dickinson M. & Pettini M., 1999, ApJ, 519, 1
- Steidel C. C., Pettini M. & Hamilton D., 1995, ApJ, 110, 2519
- Sugiyama N., 1995, ApJS, 100, 281
- Sutherland W. et al., 1999, MNRAS, 308, 289
- Tadros H. & Efstathiou G., 1996, MNRAS, 282, 1381
- Tadros H., Efstathiou G. & Dalton G., 1998, MNRAS, 296, 995
- Wilson G., Kaiser N. & Luppino G. A., 2001, ApJ, 556, 601
- Yee H. K. C., Morris S. L., Lin H., Carlberg R. G., Hall P. B., Sawicki M., Patton D. R., Wirth G. D., Ellingson E. & Shepherd C. W., 2000, ApJS, 129, 475